STRUCTURAL SCIENCE
CRYSTAL ENGINEERING
MATERIALS

ISSN: 2052-5206
journals.iucr.org/b

Pressure-dependent X-ray diffraction of the multiferroics RMn_2O_5

Wei Peng, Victor Balédent, Marie-Bernadette Lepetit, Antoine Vaunat, Elisa Rebolini, Martha Greenblatt and Pascale Foury-Leylekian

Acta Cryst. (2019). B**75**, 687–696

Acta Cryst B
STRUCTURAL SCIENCE
CRYSTAL ENGINEERING
MATERIALS

ISSN 2052-5206

Pressure-dependent X-ray diffraction of the multiferroics $R\mathrm{Mn_2O_5}$

Wei Peng,[a]‡ Victor Balédent,[a] Marie-Bernadette Lepetit,[b,c] Antoine Vaunat,[a] Elisa Rebolini,[c] Martha Greenblatt[d] and Pascale Foury-Leylekian[a]*

[a]Laboratoire de Physique des Solides, CNRS, Université Paris-Sud, Université Paris-Saclay, 91405 Orsay cedex, France, [b]CNRS, Institut Néel, F-38000 Grenoble, France, [c]Institut Laue–Langevin, 72 avenue des Martyrs, 38042 Grenoble, France, and [d]Department of Chemistry and Chemical Biology, Rutgers, State University of New Jersey, Piscataway, NJ 08854, USA. *Correspondence e-mail: pascale.foury@u-psud.fr

Received 3 March 2019
Accepted 31 May 2019

Edited by S. Parsons, University of Edinburgh, Scotland

‡ Current address: Max Planck Institute for Chemical Physics of Solids, Nöethnitzer Strasse 40, 01187 Dresden, Germany.

Keywords: multiferroics; high pressure; structure evolution with pressure; exchange interactions.

CCDC reference: 1919948

Supporting information: this article has supporting information at journals.iucr.org/b

The room-temperature structural properties of the $R\mathrm{Mn_2O_5}$ multiferroics have been investigated under pressure, using powder X-ray scattering and density functional theory (DFT) calculations. It was possible to determine the lattice parameters and the main atomic positions as a function of pressure. Good agreement was observed between the X-ray and DFT results for most of the determined crystallographic data. From the DFT calculations, it was possible to infer the pressure evolution of the exchange interactions, and this analysis led to the conclusion that the onset of the $q = (\frac{1}{2}, 0, \frac{1}{2})$ magnetic structure under pressure is related to the increase in the J_1 super-exchange terms (due to the reduction in the Mn—O distances) compared with the Mn—R exchange interactions. In addition, the 1D antiferromagnetic character of the compounds should be reinforced under pressure.

1. Introduction

Multiferroics are compounds possessing more than one type of ferroic (or antiferroic) order such as ferromagnetism, ferroelectricity, ferroelasticity or ferrotoroidicity (Eerenstein *et al.*, 2006). Magnetoelectric multiferroics [exhibiting the coexistence of magnetism, ferroelectricity and magneto-electric coupling (MEC)] have received a lot of attention, both for their unusual physical properties and their potential technological applications. Indeed, they open the possibility of achieving a cross control of electric and magnetic properties (Kimura *et al.*, 2003; Lottermoser *et al.*, 2004; Spaldin, 2005).

Among the magnetoelectric multiferroics, the $R\mathrm{Mn_2O_5}$ family (R = rare earth, Bi or Y) is exceptional as two members of the series [Tb (Hur *et al.*, 2004*a*), Gd (Lee *et al.*, 2013)] can achieve complete polarization reversal by the application of a magnetic field. A common feature of these compounds is the presence of complex magnetic orders, originating from their strongly frustrated spin systems. Unlike many multiferroic compounds, the microscopic origin of the magnetoelectric coupling cannot be attributed to the Dzyaloshinskii–Moriya interaction (Kimura, 2007), which is incompatible with the nearly collinear character of the $R\mathrm{Mn_2O_5}$ spin orders. Instead an 'exchange–striction' mechanism, first proposed by Chapon *et al.* (2006), was recently established (Yahia *et al.*, 2017). In addition, the microscopic mechanism of the atomic displacements responsible for the polarization was unveiled (Yahia *et al.*, 2018).

As claimed in a recent article (Balédent *et al.*, 2015), the $R\mathrm{Mn_2O_5}$ compounds crystallize in the ferroelectric *Pm* space group even at room temperature. Their *Pm* structure only

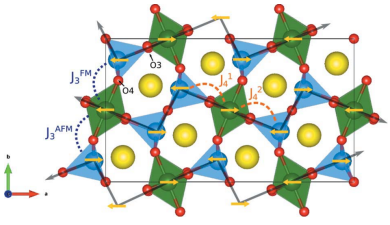

differs from the averaged non-polar *Pbam* orthorhombic one (considered generally) by weak deformations. The structure is composed of $Mn^{4+}O_6$ octahedra and $Mn^{3+}O_5$ square-based pyramids (see Fig. 1). In the *ab* plane, the edge-sharing $Mn^{4+}O_6$ octahedra and $Mn^{3+}O_5$ pyramids form pentagons.

In the *Pbam* space group there are three inequivalent antiferromagnetic (AFM) super-exchange interactions between Mn ions in the *ab* plane: J_3 and J_4 for the Mn^{3+}–Mn^{4+} dimers, and J_5 between two Mn^{3+} nearest-neighbor ions (see Fig. 1). The J_4 and J_5 interactions form two AFM zigzag chains per unit cell along the *a* axis (see Fig. 9). The J_3 interactions couple these chains, but their effect essentially cancels out due to magnetic frustration. The polarization sets in order to release this frustration. Indeed, the atomic displacements associated with the polarization differentiate the J_3 values between ferromagnetically and antiferromagnetically ordered Mn ions. Along the *c* axis, there are two different AFM Mn^{4+}–Mn^{4+} exchange interactions between the Mn^{4+} layers [Fig. 1(*b*)], J_1 (through the R^{3+} layers) and J_2 (through the Mn^{3+} layers). The J_2 interactions are strongly frustrated, as the two Mn^{4+} ions are part of four Mn^{4+}–Mn^{3+}–Mn^{4+} triangles, involving two J_4 Mn^{3+}–Mn^{4+} interactions and two J_3 Mn^{3+}–Mn^{4+} interactions. Hence, the magnetic ordering between the two Mn^{4+} ions (J_2) is always ferromagnetic (FM) (Petit *et al.*, 2013; Radaelli & Chapon, 2008). For J_1, the situation is more complex and the ordering depends strongly on the rare earth (its magnetism and number of 4*f* electrons) as well as on the detailed structural parameters. In particular, it is greatly affected by the distances and angles between the cations and O atoms involved in the super-exchange couplings. These multiple exchange interactions are difficult to calculate with *ab initio* methods because of the large number of open 3*d* and 4*f* shells and the strong spin–orbit coupling of the 4*f* elements. They have been evaluated experimentally using inelastic neutron scattering in RMn_2O_5 (*R* = Y and Tb). However, such experiments, requiring large single crystals, can not easily be generalized to other members of the series or to measurements under pressure.

Upon cooling, the RMn_2O_5 compounds usually undergo a cascade of magnetic and ferroelectric phase transitions. In most systems, one finds a first phase transition (at $T_N \simeq 40$ K) between the paramagnetic–paraelectric (PM/PE) state and an incommensurate magnetically ordered one (ICM1/PE), and then the magnetic ordering locks into a commensurate order at $T_{c1} \simeq 35$ K. This order coincides with the emergence of a ferroelectric polarization along the *b* axis (CM/FE1). Upon further cooling, below $T_{c2} \simeq 25$ K, a re-entrance of an incommensurate magnetic phase (ICM2) is observed, usually with a sharp change in the polarization (LT-ICM2/FE2). Finally, the rare earth moments order at low temperature. Depending on the nature of *R*, the very existence of the different phases differs, as well as their propagation vectors. This is also the case for the magnetoelectric properties. The dependence of the electric polarization on *R* is presented in Fig. 2. The strong variations in the electric polarization cannot be explained by the simple chemical-pressure effect associated with the difference in the R^{3+} ionic radii. $GdMn_2O_5$ exhibits the strongest electric polarization of the series and even one of the strongest among spin-induced multiferroics (3600 μC cm^{-2}; Lee *et al.*, 2013). As for $LaMn_2O_5$ and $PrMn_2O_5$, they are non-ferroelectric (Doubrovsky *et al.*, 2012). The magnetic order can even be commensurate over the whole range of temperature, as reported for $LaMn_2O_5$ (Muñoz *et al.*, 2005), $BiMn_2O_5$ (Muñoz *et al.*, 2002) and $PrMn_2O_5$ (Doubrovsky *et al.*, 2012), or incommensurate over the whole range of temperature as in $NdMn_2O_5$ (Chattopadhyay *et al.*, 2016). In these complex systems, the large effect of small variations in the interatomic distances and angles on the super-exchange integrals induces a strong dependence of the multiferroic properties on external factors. Indeed, an enhanced polarization has been observed under pressure (de la Cruz *et al.*, 2006; Chaudhury *et al.*, 2008) in the RMn_2O_5 (*R* = Tb, Ho and Y) compounds and it has been associated with a new pressure-induced magnetic phase, recently shown by neutron measurements on Y (Deutsch *et al.*, 2015; Kozlenko *et al.*, 2015), Tb (Deutsch *et al.*, 2018) and $PrMn_2O_5$ (Peng *et al.*, 2017).

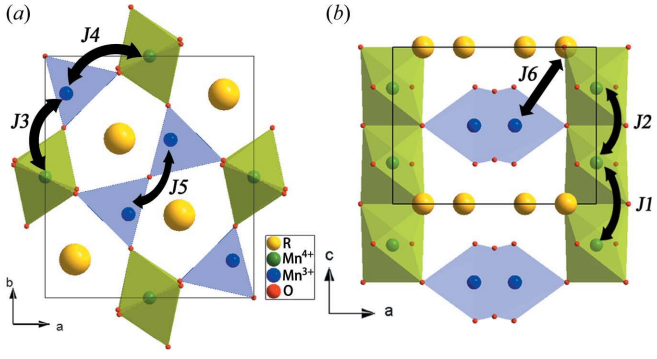

Figure 1
Projections of the RMn_2O_5 crystal structure along (*a*) the *c* axis and (*b*) the *b* axis. The different J_i exchange interactions are indicated by heavy black arrows.

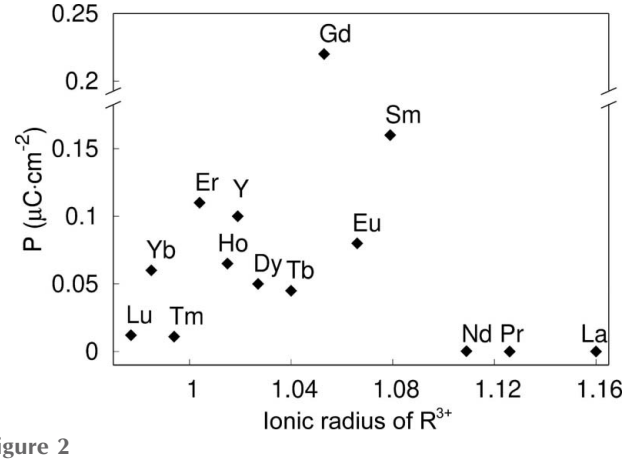

Figure 2
The dependence of the electric polarization of RMn_2O_5 at ambient pressure as a function of the ionic radius of R^{3+}. Data taken from Koyata & Kohn (1997), Kagomiya & Kohn (1998), Fujita & Kohn (1998), Hur *et al.* (2004*b*), Higashiyama *et al.* (2005), Kobayashi *et al.* (2005), Chaudhury *et al.* (2008), Fukunaga *et al.* (2011), Lee *et al.* (2013), Zhao *et al.* (2014) and Chattopadhyay *et al.* (2016).

In this paper, we present a systematic study of the structural properties of the RMn$_2$O$_5$ (R = Pr, Nd, Sm, Gd, Tb and Dy) family under pressure. From powder X-ray diffraction experiments at room temperature, we were able to obtain the lattice parameters and position information of the R^{3+}, Mn^{3+} and Mn^{4+} ions. We also performed first-principles calculations to obtain the full structural information as a function of pressure. With the assistance of the optimized structural parameters, we are able to deduce the evolution of the exchange interactions with pressure and explain the effect of pressure on the multiferroic properties.

2. Measurements setup

The measurements presented in this paper were performed using high-purity polycrystalline samples of RMn$_2$O$_5$ (R = Pr, Nd, Sm, Gd, Tb and Dy). They were synthesized from a precursor-based flux, following the method described by Popov *et al.* (2000). Powder X-ray diffraction experiments under pressure were carried out at the Laboratoire de Physique des Solides (Université Paris Sud, Orsay, France). The X-ray wavelength was 0.71 Å. The setup was developed recently. It consists of a multilayer mirror monochromator with a focalization of 1:1. The cell used was a diamond-anvil pressure cell and the transmitting liquid was silicone oil. The pressure was modified *in situ* using He gas pressure applied on a metallic membrane. The pressure on the sample volume was estimated by measuring the fluorescence wavelength of a ruby placed inside the sample volume. The measurements were performed at room temperature (∼293 K) from ambient pressure to about 9 GPa. The scattered intensities were recorded on a MAR345 detector, allowing a large wavevector range and a high resolution. The diffractograms obtained were refined using the *FULLPROF* program (Rodríguez-Carvajal, 1993).

The refinements were performed at ambient pressure using the atomic positions of Alonso *et al.* (1997), Kagomiya *et al.* (2002) and Wilkinson *et al.* (1981) as a starting point. They were performed in the *Pbam* average space group because the atomic deviations of the real *Pm* structure cannot be detected in powder X-ray measurements. We first refined the lattice parameters and then the positions of the R^{3+}, Mn^{3+} and Mn^{4+} ions. Finally, we tried to refine all the oxygen atomic positions. However, due to the lack of sensitivity of X-rays to light atoms such as oxygen, we were not able to obtain a reliable refinement of their atomic positions. We thus fixed their positions to the values found in the literature under ambient pressure (space group *Pbam*).

3. First-principles calculations

The calculations were done using the density functional formalism with the *CRYSTAL* code (Dovesi *et al.*, 2014). The functional used was the PBE functional optimized for solids (Perdew *et al.*, 2008). The rare earth atoms were treated using a relativistic-core effective potential from the Stuttgart–Köln group (Dolg *et al.*, 1989, 1993) and the associated basis set (Yang & Dolg, 2005) of valence 3-ζ quality, adapted for solid-state calculations. The Mn and O atoms were treated using the Peintinger *et al.* (2013) all-electron basis set of 3-ζ quality. We performed a full geometry optimization for the DyMn$_2$O$_5$ and GdMn$_2$O$_5$ compounds as a function of applied pressure within the *Pm* space group in a $2a \times b \times c$ unit cell, and the $(\frac{1}{2}, 0, 0)$ AFM ordering for the manganese spins. The pressure was applied as an additional term in the stress tensor (Doll, 2010):

$$\sigma_{ij}^{\text{total}} = \sigma_{ij} + \sigma_{ij}^{\text{applied}} \quad \text{with} \quad \sigma_{ij} = \frac{1}{V}\frac{\partial E}{\partial \varepsilon_{ij}}, \tag{1}$$

where E is the density functional theory (DFT) total energy, ε_{ij} are the elements of the symmetric strain tensor and V is the cell volume. Inverting these equations, one obtains the modified gradient as a function of the cell parameters, a_{ij}, to be used in the minimization procedure,

$$\left(\frac{\partial E}{\partial a_{ij}}\right)^{\text{total}} = \frac{\partial E}{\partial a_{ij}} + V\sum_{m=1}^{3}\sigma_{jm}^{\text{applied}}a_{mi}. \tag{2}$$

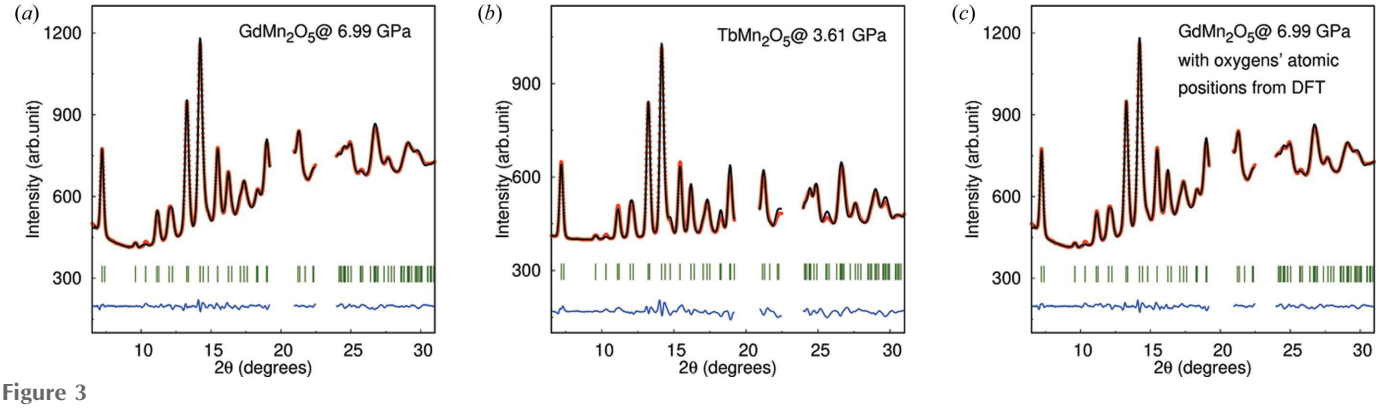

Figure 3
Refinements of (*a*) GdMn$_2$O$_5$ at 6.99 GPa, (*b*) TbMn$_2$O$_5$ at 3.61 GPa and (*c*) GdMn$_2$O$_5$ at 6.99 GPa, with fixed O atomic positions from DFT calculations. The experimental data are in red, the calculated profile in black and their difference in blue. The green ticks refer to the nuclear reflections. The peaks of the gasket have been excluded.

Table 1
Refined parameters of $GdMn_2O_5$ at different pressures.

λ = 0.71 Å.

	P (GPa)								
	0	0.78	1.56	2.46	3.51	4.8	5.91	6.99	6.99 (DFT)
Parameters									
a (Å)	7.377 (8)	7.365 (3)	7.350 (6)	7.34 (10)	7.292 (9)	7.285 (2)	7.263 (6)	7.245 (8)	7.245 (2)
b (Å)	8.557 (9)	8.553 (2)	8.545 (2)	8.537 (9)	8.505 (4)	8.513 (3)	8.502 (8)	8.494 (7)	8.493 (3)
c (Å)	5.694 (8)	5.691 (2)	5.685 (3)	5.678 (9)	5.656 (7)	5.660 (9)	5.655 (2)	5.649 (7)	5.649 (4)
Refinement									
χ^2	0.039	0.054	0.091	0.102	0.044	0.062	0.054	0.034	0.035
R_p	0.0676	0.0633	0.0793	0.0929	0.0499	0.0633	0.0586	0.0419	0.0429
R_{wp}	0.0560	0.0545	0.0721	0.0854	0.0519	0.0637	0.0592	0.0440	0.0448
R_{exp}	0.2822	0.2341	0.2385	0.2674	0.2466	0.2555	0.2536	0.2377	0.2379
R_{Bragg}	0.0380	0.0369	0.0349	0.0298	0.0129	0.0290	0.03168	0.0132	0.0154

4. Results

We refined the various structures as a function of pressure. The refinements at high pressure were of high quality for the compounds with *R* = Gd, Pr and Sm. As an example, the refinement for $GdMn_2O_5$ at 6.99 GPa is shown in Fig. 3(*a*) and demonstrates the very good agreement between the data (red points) and the calculated intensity (black line). However, in the case of the compounds with *R* = Dy, Tb and Nd, the refinements were difficult. The peak intensities at medium-high angles of their high-pressure diffractograms were not correctly fitted. The main reason was the frequent peak overlaps due to peak broadening. Such broadening is frequently observed due to the effect of strain. An additional difficulty could come from a preferred orientation effect under pressure. We thus limited our analysis to pressures below 4 GPa, for which the refinements were of good quality and reliable, as shown in Fig. 3(*b*) for $TbMn_2O_5$ at 3.61 GPa. The results of the refinements are given for $GdMn_2O_5$ as a function of pressure in Tables 1 and 2. The results for the other compounds are given in the supporting information.

In order to analyze our experimental data, we performed geometry optimizations as a function of pressure using DFT calculations for two compounds of the series, *R* = Dy, Gd. The optimization was done in the CM phase [$k = (\frac{1}{2}, 0, 0)$] which corresponds to the ground state even under pressure. We used the *Pm* space group for the calculations, thus allowing a possible polarization to take place. To demonstrate that fixing the O atomic positions to their ambient-pressure positions does not bias the refined parameters, we refined the high-pressure (6.99 GPa) data with the O atomic positions from the DFT-optimized calculation. The refinement is illustrated in Fig. 3(*c*). The refined parameters are similar to those we obtained when fixing the O atomic positions to their ambient-pressure positions (Tables 1 and 2).

The relative pressure evolution of the unit-cell parameters with respect to their ambient-pressure values is shown in Fig. 4 for the various members of the RMn_2O_5 series. Fig. 5 presents the relative pressure evolution of the unit-cell parameters deduced from our calculations. Comparison with the experimental curves shows excellent agreement. In both experimental (Fig. 4) and theoretical (Fig. 5) curves we can observe a

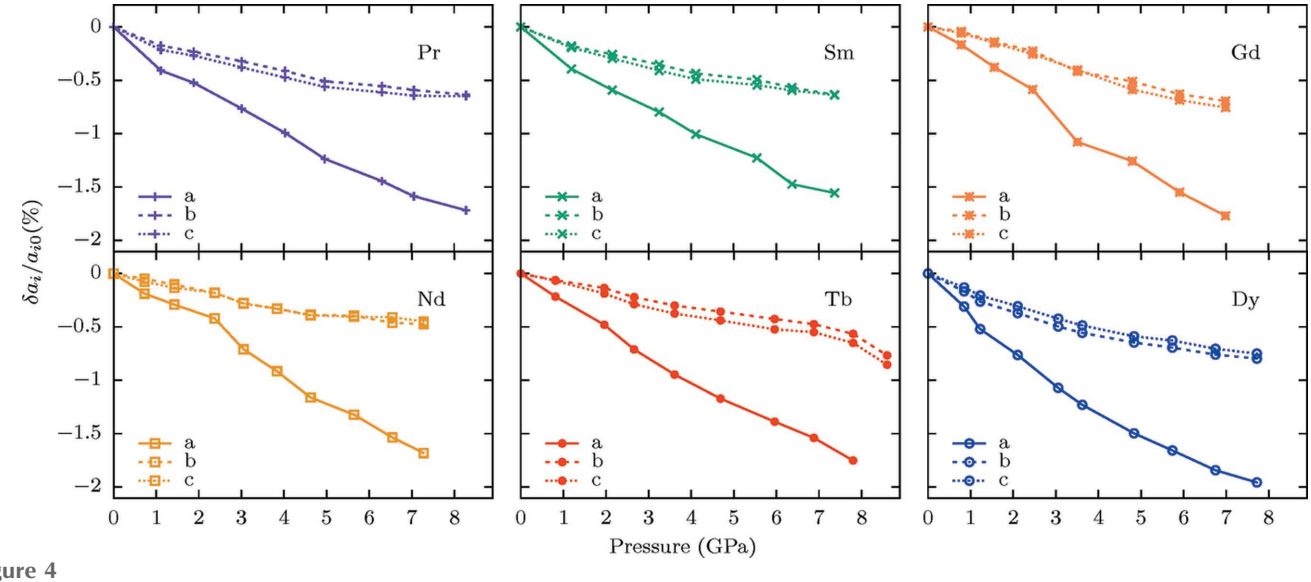

Figure 4
Measured compressibility of the unit-cell parameters $[(a_i - a_{i0})/a_{i0}]$ with respect to their ambient-pressure values, a_{i0}. Note that, for the sake of clarity, the data related to a given R^{3+} compound are always represented with the same color in all the figures of this paper.

Table 2
Refined atomic parameters and isotropic displacement (temperature) parameters (in Å^2) for $GdMn_2O_5$ at different pressures.

Pressure (GPa)	Atom	*x*	*y*	*z*	*B*
0	Gd	0.1391 (6)	0.1717 (5)	0	0.0049 (5)
	Mn1	0	0.5	0.2419 (0)	0.0045 (2)
	Mn2	0.4039 (4)	0.3535 (7)	0.5	0.0095 (8)
	O1	0	0	0.2697 (2)	0.005
	O2	0.1526 (1)	0.4486 (1)	0	0.005
	O3	0.1454 (2)	0.4356 (1)	0.5	0.005
	O4	0.3994 (8)	0.2076 (9)	0.2450 (1)	0.005
0.78	Gd	0.1386 (5)	0.1714 (9)	0	0.0041 (2)
	Mn1	0	0.5	0.2398 (3)	0.0040 (1)
	Mn2	0.4046 (0)	0.3544 (2)	0.5	0.0075 (2)
1.56	Gd	0.1376 (3)	0.1716 (5)	0	0.0039 (8)
	Mn1	0	0.5	0.2414 (4)	0.0036 (9)
	Mn2	0.4067 (4)	0.3567 (0)	0.5	0.0065 (7)
2.46	Gd	0.1373 (8)	0.1706 (7)	0	0.0037 (1)
	Mn1	0	0.5	0.2410 (2)	0.0030 (0)
	Mn2	0.4114 (9)	0.3590 (0)	0.5	0.0064 (2)
3.51	Gd	0.1446 (5)	0.1705 (1)	0	0.0078 (6)
	Mn1	0	0.5	0.2439 (5)	0.0067 (5)
	Mn2	0.4164 (7)	0.3595 (8)	0.5	0.0074 (3)
4.80	Gd	0.1436 (0)	0.1715 (5)	0	0.0093 (2)
	Mn1	0	0.5	0.2427 (9)	0.0075 (7)
	Mn2	0.4164 (8)	0.3612 (8)	0.5	0.0087 (3)
5.91	Gd	0.1434 (2)	0.1719 (8)	0	0.0102 (8)
	Mn1	0	0.5	0.2452 (8)	0.0092 (3)
	Mn2	0.4154 (4)	0.359 (9)	0.5	0.0112 (5)
6.99	Gd	0.1433 (9)	0.1739 (0)	0	0.0135 (1)
	Mn1	0	0.5	0.2461 (3)	0.0123 (7)
	Mn2	0.4171 (6)	0.351 (9)	0.5	0.0142 (9)
6.99, DFT	Gd	0.1426 (6)	0.1735 (5)	0	0.0095 (3)
	Mn1	0	0.5	0.2446 (5)	0.0102 (5)
	Mn2	0.4173 (9)	0.352 (0)	0.5	0.0117 (3)

strong anisotropy between the curve related to the lattice parameter *a* and those for *b* and *c*. The compressibility along the *a* direction at 9 GPa is twice that along the *b* and *c* directions (which are similar), indicating that the structure is softer along the *a* direction. Such behavior is observed for all the measured compounds, as well as for the Y, Bi and Ho compounds, as can be seen in the reports by Kozlenko *et al.* (2015) and Grzechnik *et al.* (2010). It is interesting to note that the *a* direction is the apical direction of the $Mn^{3+}O_5$ pyramids. Comparing the lattice compressibility with the effect of temperature presented by Doubrovsky *et al.* (2012), not only is the effect of the external pressure on the structural properties much stronger than the effect of temperature, but also the *b* and *c* directions behave differently as a function of temperature, while their behavior is very similar under pressure. This could explain the strong modifications of the multiferroic properties under pressure observed, for example, in $PrMn_2O_5$ (Peng *et al.*, 2017).

The relative evolution of the unit-cell volume as a function of pressure is presented in Fig. 6. The curves were fitted by the equation of state (EoS) provided below [equation (3)], which was developed by Rault (2014):

$$V - V^* = (V_0 - V^*)\frac{P^*}{P + P^*},$$
$$B_0 = P^*\frac{V_0}{V_0 - V^*}, \qquad (3)$$
$$B_0' = \frac{V_0 + V^*}{V_0 - V^*},$$

with $V_0(T)$ being the volume at $P = 0$, V^* the hard-core volume independent of P and T, P^* the characteristic pressure, B_0 the zero-pressure bulk modulus and B_0' the pressure derivative of the bulk modulus. The fitted parameters V^*, P^*, B_0 and B_0' are listed in Table 3. The B_0 and B_0' values are very similar for the various compounds, and comparable with the values already published for $HoMn_2O_5$ and $BiMn_2O_5$ (Grzechnik *et al.*, 2010), and YMn_2O_5 (Kozlenko *et al.*, 2015). The relative pressure dependence of the compressibility of $PrMn_2O_5$, $SmMn_2O_5$ and $DyMn_2O_5$ shows a general behavior with large B_0' values (~30;

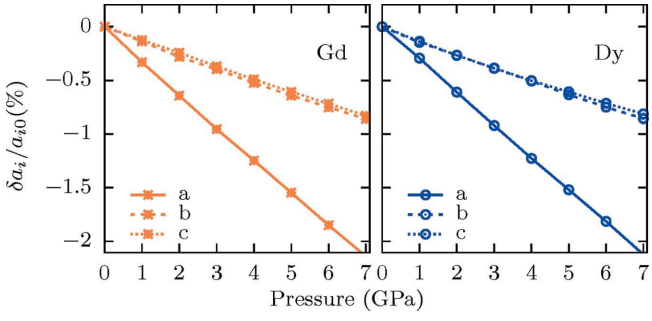

Figure 5
Compressibility of the unit-cell parameters $[(a_i - a_{i0})/a_{i0}]$ of $GdMn_2O_5$ and $DyMn_2O_5$ with respect to their ambient-pressure values, a_{i0}, calculated by DFT.

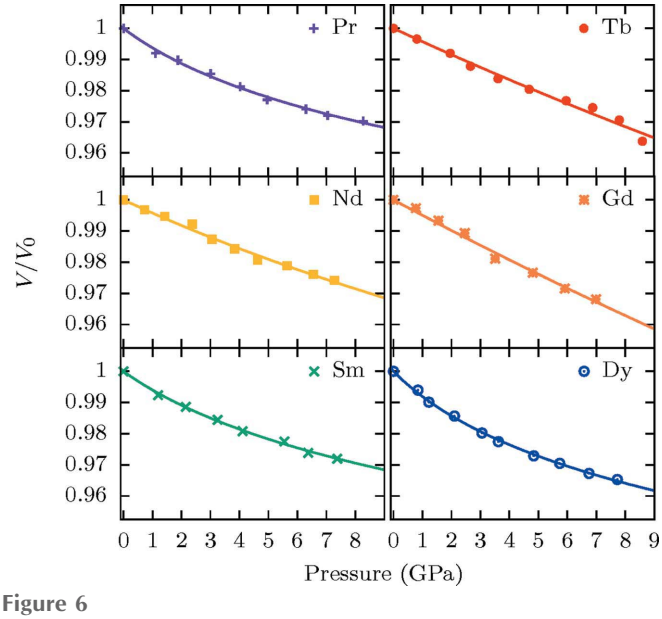

Figure 6
The relative pressure dependence of the unit-cell volume V/V_0 for the RMn_2O_5 compounds with respect to their ambient-pressure values. The solid lines show the fits using the EoS from Rault (2014).

Fig. 6). Their shape is similar to that mentioned by Rault (2014). For $TbMn_2O_5$ and $GdMn_2O_5$, the B_0' values are smaller (~3–4) and the relative pressure dependence is nearly linear. This shows that the pressure is not high enough for these compounds, thus only the early stage of the general behavior appears. At higher pressure, we expect a general behavior similar to the other compounds. As for $NdMn_2O_5$, it has an intermediate behavior with pressure.

5. Discussion

From our refinements, we extracted the pressure evolution of the atomic positions of the R^{3+}, Mn^{3+} and Mn^{4+} heavy ions. Using the software *Amplimodes* of the Bilbao server (Orobengoa *et al.*, 2009; Perez-Mato *et al.*, 2010), we compared their atomic positions with their values at ambient pressure. The amplitudes of the obtained atomic displacements are represented in Fig. 7.

Firstly, for all members of the series except $GdMn_2O_5$, the atomic displacements as a function of the pressure are weak and nearly monotonic. The maximum variations in the atomic displacements related to the heavy R^{3+} ions are always smaller than 0.05 Å and mostly along the *a* direction. The displacements of the Mn^{3+} ions remain within the *ab* plane, essentially along **a**, *i.e.* the apical direction of the pyramids. X-ray measurements under pressure performed on $HoMn_2O_5$ and $BiMn_2O_5$ single crystals (Grzechnik *et al.*, 2010) corroborated our results and obtained relative displacements between 0 and 7 GPa of 0.04 Å for the Mn^{3+} ions in $BiMn_2O_5$ and 0.03 Å for Ho^{3+} in $HoMn_2O_5$. It is important to mention that the O-atom displacements obtained by Grzechnik *et al.* (2010) are very large (0.15 Å), which makes them not fully reliable and indicates the difficulty in accurately measuring the O-atom positions using X-ray diffraction.

Secondly, in the compounds with R = Dy, Gd, Nd, the atomic displacements deduced from our measurements can reach a value close to 0.1 Å for the Mn^{3+} ions. This is surprisingly high. However, it is obvious that the Mn contribution to the X-ray pattern is very small compared with that of the R atom, which hides the Mn input and reduces the accuracy of the determination of the Mn positions. Nevertheless, strong atomic displacements are only observed for the Mn^{3+} ions and not for the Mn^{4+} ones. This could be an indication of a real effect associated with a structural transition involving mainly the Mn^{3+} ions and observed only in the Dy, Gd and Nd compounds. In order to check these results accurately, we performed numerous refinements of the data under pressure starting from various initial models. We also refined the data in the *Pm* space group using symmetry constraints to achieve convergence. Finally, we checked the correlations between atomic position parameters to exclude the possibility of erroneous atomic shifts. All the refinements performed led to a similar structure at 7 GPa, evidencing Mn^{3+} displacements of 0.1 Å from the ambient-pressure positions. Furthermore, if the Mn^{3+} are restrained to stay roughly around their ambient-pressure position, the refinement is not good.

Table 3
The fitted values of B_0 and B_0' for the RMn_2O_5 compounds.

V_0 is the volume at $P = 0$, V^* is the hard-core volume independent of P and T, P^* is the characteristic pressure, B_0 is the zero-pressure bulk modulus and B_0' is the pressure derivative of the bulk modulus.

R	V_0 (cm^3)	V^* (cm^3)	P^* (GPa)	B_0 (GPa)	B_0'
Pr	901.253	841.612	9.860	148.998	29.222
Nd	891.629	750.974	36.315	230.209	11.678
Sm	875.729	815.798	10.685	156.141	28.224
Gd	865.704	429.171	100.747	199.797	2.966
Tb	861.401	529.156	89.686	232.527	4.185
Dy	850.993	790.291	8.026	112.524	27.038
Ho†				173	4
Bi†				138	4
Y‡				192	3

† Grzechnik *et al.* (2010). ‡ Kozlenko *et al.* (2015).

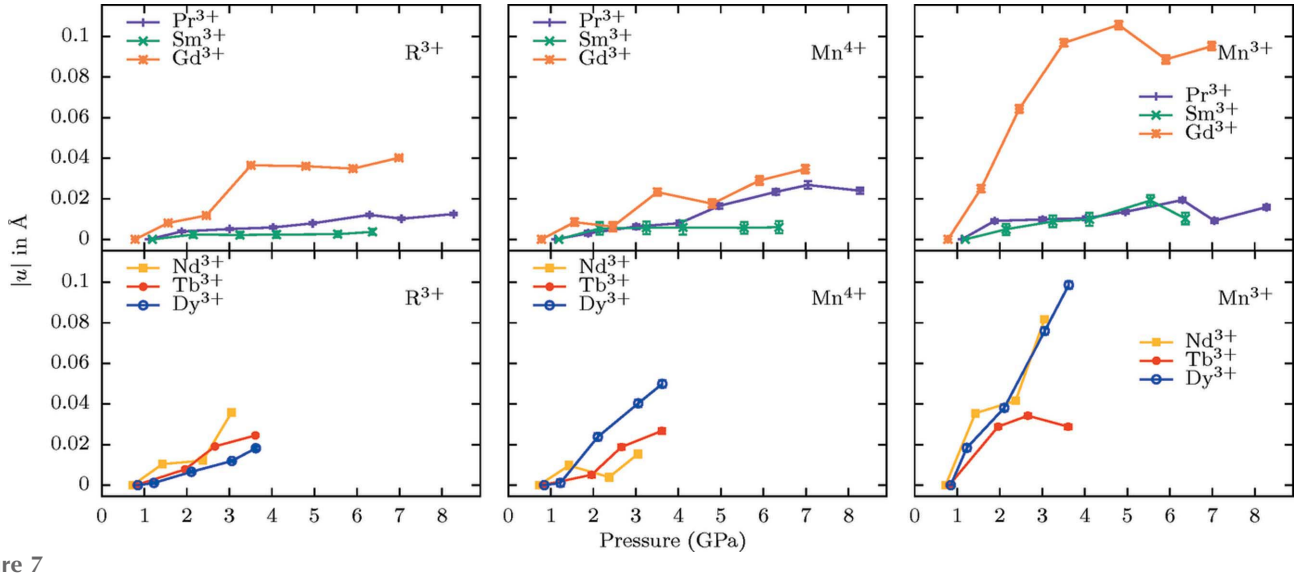

Figure 7
The measured ionic displacements $|u|$ of the RMn_2O_5 compounds (R = Pr, Sm, Gd, Nd, Tb, Dy) with respect to their initial pressure values, for R^{3+} (left), Mn^{4+} (middle) and Mn^{3+} (right). The error bars are within the width of the points.

In the case of $GdMn_2O_5$, for which our refinements were of high quality and thus very reliable, the atomic positions of Gd^{3+} present a step-like anomaly at 3 GPa, in addition to a strong Mn^{3+} displacement. It is interesting to note that the pressure evolution of the unit-cell parameter *a* also presents a weak anomaly at 3 GPa (Fig. 4). The possibility of this anomaly being associated with a phase transition will be investigated in future work.

To analyze our experimental data further, we compared our results with DFT calculations performed on the Gd and Dy compounds. For both compounds we observe excellent agreement between the calculated and measured pressure evolutions of the compressibility $\delta a_i/a_{i0}$ (Fig. 5). Fig. 8 reports the measured and calculated relative displacements (with respect to the initial pressure value) for the heaviest ions, namely Gd^{3+} and Dy^{3+}. One sees immediately that they are close at low pressure, even if the calculated values are always slightly smaller than the experimental ones. It is indeed known that the PBE functional usually underestimates atomic displacements (Mori-Sánchez *et al.*, 2008). However, in the case of $GdMn_2O_5$, the calculated Gd^{3+} displacements do not present any anomaly at 3 GPa. These results support the hypothesis of a phase transition around 3 GPa, as the DFT calculations are bounded by symmetry within a specific phase. If there is a phase transition between the $(\frac{1}{2}, 0, 0)$ magnetic phase (the ground state at low pressure) and the $(\frac{1}{2}, 0, \frac{1}{2})$ one (the ground state at higher pressure for all the compounds of the series) then, due to its restriction to the $(\frac{1}{2}, 0, 0)$ phase, our DFT calculations cannot account for it. Indeed, we did not allow the doubling of the unit cell along the *c* axis necessary to reach a $(\frac{1}{2}, 0, \frac{1}{2})$ propagation vector.

The only reliable information for the positions of the light O atoms comes from the DFT calculations. From this information, as well as from the positions of the Mn ions as a function of pressure, it is possible to infer information on the pressure evolution of the exchange interactions in the system. This information is essential to understand the multiferroic properties under pressure.

Let us recall that ligand-bridged effective exchange integrals are the sum of three terms: the direct exchange (J_d, always FM), the through-space or direct super-exchange (J_{sd}, always AFM, usually very small) and the through-bridge super-exchange term, mediated by the ligands ($J_{3,sb}$, always AFM). Unless symmetry-forbidden, the latter term is usually the dominant one. A detailed analysis of the different super-exchange terms in the magnetic integrals of the RMn_2O_5 family can be found in the supporting information.

We will focus first on the exchange interactions along the *c* axis, namely J_1 and J_2. Indeed, one of the main effects of increasing pressure is the onset of magnetic ordering with a unique $(\frac{1}{2}, 0, \frac{1}{2})$ propagation vector for all compounds of the family. For the two magnetic interactions along the *c* direction, the super-exchange terms are similar and do not depend on the $Mn^{4+}—O—Mn^{4+}$ angles, but only on the $Mn^{4+}—O$ distances (see supporting information). The Mn—O distances vary in a quasi-linear way as a function of pressure (not shown). One can thus expect an associated quasi-linear increase in the two J_i (i = 1, 2) values by a few percent. As far as J_2 is concerned, this increase should not qualitatively modify the ferromagnetic ordering of the Mn^{4+} ions on each side of the Mn^{3+} ones, as this ordering is imposed by the frustration between the J_2 AFM exchange and the four J_3 and J_4 AFM exchanges, which couple the two Mn^{4+} ions via Mn^{3+} along the *c* direction. The J_1 magnetic exchange is in competition with the Mn^{4+}–R^{3+} magnetic exchanges, J_6, which can be expected to be small. An increase in J_1 with respect to the interactions between the Mn^{4+} and the rare earth ions could thus modify the propagation vector of the magnetic structure along the *c* axis. Indeed, an increase in J_1 favors an AFM ordering between neighboring Mn^{4+} ions that is a $\frac{1}{2}$ component along the *c* axis. This could lead to the PCM phase, which has recently been discovered under pressure in the *R* = Y, Tb, Pr and Dy compounds (Deutsch *et al.*, 2015, 2018; Peng *et al.*, 2017). It is important to note that compounds with non-magnetic R^{3+} ions such as in $BiMn_2O_5$ (Muñoz *et al.*, 2002) do not encounter frustration due to the J_6 interactions. In the latter, the AFM ordering between the Mn^{4+} ions through J_1 is simply due to the super-exchange interaction Mn^{4+}–O–Mn^{4+}, which leads to a component of the propagation wave vector of $\frac{1}{2}$.

Let us now concentrate on the J_3 interactions. A picture of the atoms involved in this interaction is given in Fig. 9. There are two different J_3 exchange interactions, one involved in an FM-ordered pair of Mn spins (labeled J_3^{FM} in Fig. 9) and one in an AFM-ordered pair (J_3^{AFM}). The two J_3 couplings are non-equivalent by symmetry in the *Pm* space group. Within the exchange–striction model, if the spins coupled by J_3 are not

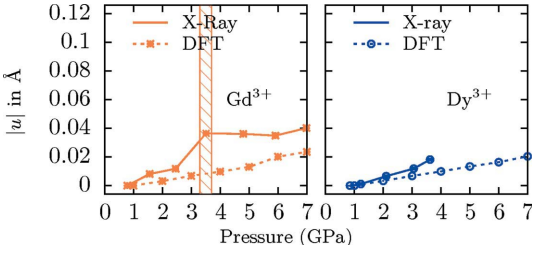

Figure 8
Comparisons of the evolution with pressure of the ionic displacements $|u|$ of Gd^{3+} and Dy^{3+} by X-ray experiments and DFT calculations, with respect to their initial pressure values.

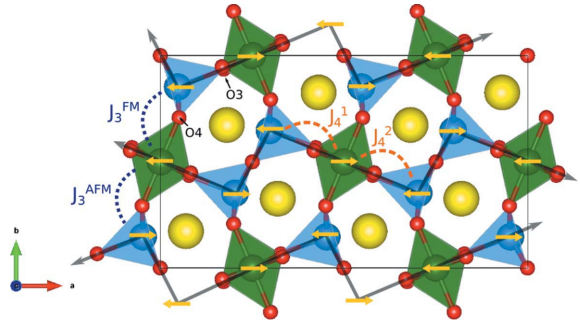

Figure 9
The different exchange interactions.

perpendicular (the J_3 term does not cancel), it is the release of the magnetic frustration over J_3 that is responsible for the onset of polarization (Blake *et al.*, 2005; Yahia *et al.*, 2018). The difference between J_3^{AFM} and J_3^{FM}, which is a consequence of the exchange–striction mechanism, is thus directly connected to the electric polarization. As detailed in the supporting information, there are three super-exchange paths to the J_3 interactions. The largest one is independent of the Mn^{3+}—O4—Mn^{4+} angle, α_3, the second largest one varies as $\cos^2\alpha_3$ and the weakest one as $\sin^2\alpha_3$. Of course, all three terms vary as a function of the Mn^{3+}—O4 and Mn^{4+}—O4 distances.

Fig. 10 shows (for the Gd and Dy compounds) the variation in the two Mn—O distances and $\cos^2\alpha_3$ as a function of applied pressure for the two J_3 interactions. The structural differences releasing the J_3 frustration and responsible for the onset of polarization can be immediately seen. Indeed, Fig. 10 clearly exhibits the Mn^{4+}—O4 distance contraction, and the Mn^{4+}—O4—Mn^{3+} angle increment, when comparing atoms that are AFM ordered and atoms that are FM ordered. Surprisingly, the Mn^{3+}—O4 distances are affected neither by the spin arrangement (FM or AFM) nor by the nature of the rare earth. Indeed, in Fig. 10, all the curves associated with the Mn^{3+}—O4 distances are identical. The quasi-linear variation in the distances and the flat evolution of the angle cosine as a function of applied pressure lead to an overall weak increase in the J_3 values. More importantly, as no significant evolution of the difference between the two J_3 interactions can be observed from these data (the curves of J_3 for AFM and FM pairs are parallel as a function of pressure), one can safely infer that the amplitude of the polarization should not be affected by pressure, at least as long as the $q = (\frac{1}{2}, 0, 0)$ phase is dominant. This is corroborated by polarization measurements performed on $GdMn_2O_5$ (Poudel *et al.*, 2015) and $DyMn_2O_5$ (de la Cruz *et al.*, 2007) indicating a pressure independence of the polarization at low temperature in the ground state corresponding to the $q = (\frac{1}{2}, 0, 0)$ magnetic phase.

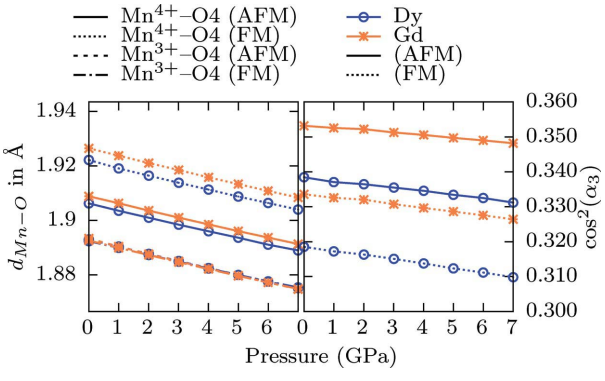

Figure 10
The variation in the structural parameters involved in the J_3 amplitudes as a function of applied pressure. The blue circles are for the $DyMn_2O_5$ compound and the orange crosses for the $GdMn_2O_5$ one. (Left) Mn^{4+}—O4 and Mn^{3+}—O4 distances (Å). (Right) $\cos^2\alpha_3$, α_3 being the Mn^{4+}—O4—Mn^{3+} angle. (AFM) refers to the geometric parameters between atoms involved in AFM-ordered Mn^{4+}–Mn^{3+} ions, while (FM) refers to the parameters between FM-ordered ones.

As can be seen in Fig. 9, there are two inequivalent J_4 couplings in the *Pm* space group. However, as the structural parameters involved in these two interactions are very similar, they will be considered identical. For J_4, there are three super-exchange paths contributing to the J_4 interaction (see supporting information). One is independent of the Mn^{4+}—O3—Mn^{3+} angle, α_4, while the other two vary, respectively, as $\sin^2\alpha_4$ and $\cos^2\alpha_4$. As the bridging O3 ion is the apical atom of the $Mn^{3+}O_5$ square pyramid, the Mn^{3+} d_{z^2} orbital pointing towards it has the largest Mn^{3+}—O3 transfer integral and is thus associated with the potentially largest contribution to J_4 ($\sin^2\alpha_4$ varying term). The variations in the structural parameters involved in J_4 are displayed in Fig. 11 as a function of pressure.

Unlike the equatorial bond of the $Mn^{3+}O_5$ pyramid involved in J_3, the apical bond involved in the J_4 interaction varies strongly with pressure due to the strong contraction of the unit-cell parameter *a*. Indeed, there is a difference of about 0.04 Å between its value at ambient pressure and that at 7 GPa. In contrast, the Mn^{4+}—O_3—Mn^{3+} angles display little distortion under pressure, despite the fact that they are along the most contracted direction (*a*). In contrast with J_3, J_4 is thus expected to present a strong relative increase under pressure, and thus one expects an increase in the 1D character of the magnetic interactions.

As for J_5, despite the fact that there are different symmetry-irreducible J_5 interactions in the polar group, all the geometric parameters involved are numerically equivalent. There is thus only one type of J_5 interaction even in the *Pm* symmetry group. As detailed in the supporting information, there are four super-paths that go in pairs. Two of them are only dependent on the Mn^{3+}—O1 distance, while the other two vary as $|\sin\alpha_5 + \sin\alpha_5'|^2$, where α_5 and α_5' are the two Mn^{3+}—O1—Mn^{3+} angles. Fig. 12 displays $|\sin\alpha_5 + \sin\alpha_5'|^2$ and the Mn^{3+}—O1 distances as a function of pressure. In fact within numerical accuracy, $\alpha_5 = \alpha_5'$ in our calculations. One can see in Fig. 12 that the distance variations are negligible ($\sim 5 \times 10^{-4}$ Å), while the angles are brought closer to 90°

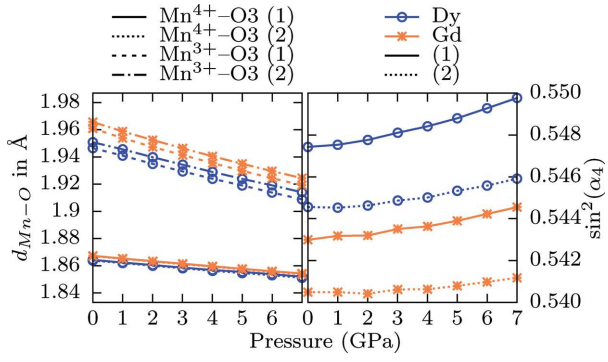

Figure 11
The variation in the structural parameters involved in the J_4 amplitudes as a function of applied pressure. The blue circles are for the $DyMn_2O_5$ compound and the orange crosses for the $GdMn_2O_5$ one. (Left) Mn^{4+}—O3 and Mn^{3+}—O3 distances (Å). (Right) $\sin^2\alpha_4$, α_4 being the Mn^{4+}—O3—Mn^{3+} angle.

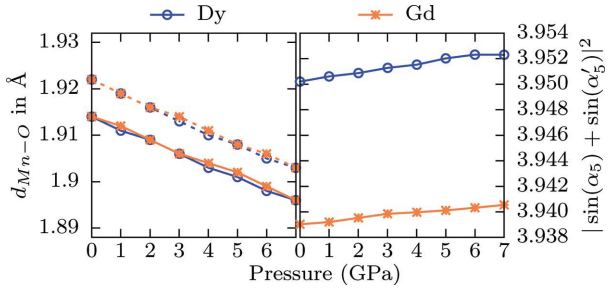

Figure 12
The variation in the structural parameters involved in the J_5 amplitudes as a function of applied pressure. The blue circles are for the $DyMn_2O_5$ compound and the orange crosses for the $GdMn_2O_5$ one.

under pressure. This should result in a very small increase in J_5 under pressure.

6. Conclusions

Using correlated powder X-ray diffraction experiments and DFT calculations, we have been able to show that the effect of external pressure up to 9 GPa on the structural properties of RMn_2O_5 multiferroics is more important than the thermal contraction from 300 K to 10 K. The evolution of the unit-cell parameters under pressure is strongly anisotropic with a softer *a* direction. Let us recall that this is the direction of the dominant magnetic interactions, resulting in a magnetic structure that can be described by weakly coupled AFM chains running along the *a* axis. From the experimental determination of the molecular volume, we were able to extract the compressibility parameters.

The refinement of our X-ray diffractograms gave indications on the positions of the heavy ions (R^{3+}, Mn^{3+} and Mn^{4+}). We have detected a possible structural transition at ∼3 GPa in $GdMn_2O_5$ that will be the subject of further work.

As the DFT calculations account well for the experimental results concerning the unit-cell parameters, as well as the atomic positions of the R^{3+} ions, we used them to obtain the missing information in our experimental investigation, namely the positions, as a function of pressure, of the light atoms such as O and, to a lesser extent, the Mn. From the calculated O and Mn positions, we extracted information concerning the evolution of the exchange interactions J_i as a function of pressure.

From this analysis we were able to infer: (i) that the electric polarization should be only slightly affected by the applied pressure as long as the ground state remains identical to the ambient-pressure one with a $(\frac{1}{2}, 0, 0)$ magnetic wavevector; and (ii) that the 1D AFM character of the magnetic structure should be reinforced. Further investigations of the pressure evolution of the structure at low temperature are in progress to confirm these findings.

The study of the structural properties of single crystals would also be very interesting to detect weaker effects such as those related to the symmetry breaking from the *Pbam* space group to the *Pm* one (Balédent *et al.*, 2015) and their evolution with pressure.

Funding information

This work was supported by the Chinese Scholarship Council project. The work of M. Greenblatt at Rutgers was supported by a grant from the US National Science Foundation (grant No. NSF-DMR 15040976). The DFT calculations were performed at the IDRIS and CRIANN computer centers (Campus France) under project Nos. 081842 and 2007013.

References

Alonso, J. A., Casais, M. T., Martínez-Lope, M. J., Martínez, J. L. & Fernández-Díaz, M. T. (1997). *J. Phys. Condens. Matter*, **9**, 8515–8526.
Balédent, V., Chattopadhyay, S., Fertey, P., Lepetit, M. B., Greenblatt, M., Wanklyn, B., Saouma, F. O., Jang, J. I. & Foury-Leylekian, P. (2015). *Phys. Rev. Lett.* **114**, 117601.
Blake, G. R., Chapon, L. C., Radaelli, P. G., Park, S., Hur, N., Cheong, S.-W. & Rodríguez-Carvajal, J. (2005). *Phys. Rev. B*, **71**, 214402.
Chapon, L. C., Radaelli, P. G., Blake, G. R., Park, S. & Cheong, S.-W. (2006). *Phys. Rev. Lett.* **96**, 097601.
Chattopadhyay, S., Balédent, V., Damay, F., Gukasov, A., Moshopoulou, E., Auban-Senzier, P., Pasquier, C., André, G., Porcher, F., Elkaim, E., Doubrovsky, C., Greenblatt, M. & Foury-Leylekian, P. (2016). *Phys. Rev. B*, **93**, 104406.
Chaudhury, R. P., dela Cruz, C. R., Lorenz, B., Sun, Y., Chu, C.-W., Park, S. & Cheong, S.-W. (2008). *Phys. Rev. B*, **77**, 220104.
dela Cruz, C. R., Lorenz, B., Sun, Y. Y., Wang, Y., Park, S., Cheong, S. W., Gospodinov, M. M. & Chu, C. W. (2007). *Phys. Rev. B*, **76**, 174106.
dela Cruz, C. R., Yen, F., Lorenz, B., Gospodinov, M. M., Chu, C. W., Ratcliff, W., Lynn, J. W., Park, S. & Cheong, S. W. (2006). *Phys. Rev. B*, **73**, 100406.
Deutsch, M., Hansen, T. C., Fernandez-Diaz, M. T., Forget, A., Colson, D., Porcher, F. & Mirebeau, I. (2015). *Phys. Rev. B*, **92**, 060410.
Deutsch, M., Peng, W., Foury-Leylekian, P., Balédent, V., Chattopadhyay, S., Fernandez-Diaz, M. T., Hansen, T. C., Forget, A., Colson, D., Greenblatt, M., Lepetit, M.-B., Petit, S. & Mirebeau, I. (2018). *Phys. Rev. B*, **98**, 024408.
Dolg, M., Stoll, H. & Preuss, H. (1989). *J. Chem. Phys.* **90**, 1730–1734.
Dolg, M., Stoll, H. & Preuss, H. (1993). *Theor. Chim. Acta*, **85**, 441–450.
Doll, K. (2010). *Mol. Phys.* **108**, 223–227.
Doubrovsky, C., André, G., Gukasov, A., Auban-Senzier, P., Pasquier, C. R., Elkaim, E., Li, M., Greenblatt, M., Damay, F. & Foury-Leylekian, P. (2012). *Phys. Rev. B*, **86**, 174417.
Dovesi, R., Orlando, R., Erba, A., Zicovich-Wilson, C. M., Civalleri, B., Casassa, S., Maschio, L., Ferrabone, M., De La Pierre, M., D'Arco, P., Noël, Y., Causà, M., Rérat, M. & Kirtman, B. (2014). *Int. J. Quantum Chem.* **114**, 1287–1317.
Eerenstein, W., Mathur, N. D. & Scott, J. F. (2006). *Nature*, **442**, 759–765.
Fujita, T. & Kohn, K. (1998). *Ferroelectrics*, **219**, 155–160.
Fukunaga, M., Sakamoto, Y., Kimura, H. & Noda, Y. (2011). *J. Phys. Soc. Jpn*, **80**, 014705.
Grzechnik, A., Tolkiehn, M., Morgenroth, W. & Friese, K. (2010). *J. Phys. Condens. Matter*, **22**, 275401.
Higashiyama, D., Miyasaka, S. & Tokura, Y. (2005). *Phys. Rev. B*, **72**, 064421.
Hur, N., Park, S., Sharma, P. A., Ahn, J. S., Guha, S. & Cheong, S.-W. (2004*a*). *Nature*, **429**, 392–395.

Hur, N., Park, S., Sharma, P. A., Guha, S. & Cheong, S.-W. (2004*b*). *Phys. Rev. Lett.* **93**, 107207.
Kagomiya, I. & Kohn, K. (1998). *Ferroelectrics*, **219**, 169–176.
Kagomiya, I., Kohn, K. & Uchiyama, T. (2002). *Ferroelectrics*, **280**, 131–143.
Kimura, T. (2007). *Annu. Rev. Mater. Res.* **37**, 387–413.
Kimura, T., Goto, T., Shintani, H., Ishizaka, K., Arima, T. & Tokura, Y. (2003). *Nature*, **426**, 55–58.
Kobayashi, S., Kimura, H., Noda, Y. & Kohn, K. (2005). *J. Phys. Soc. Jpn*, **74**, 468–472.
Koyata, Y. & Kohn, K. (1997). *Ferroelectrics*, **204**, 115–124.
Kozlenko, D. P., Dang, N. T., Kichanov, S. E., Lukin, E. V., Pashayev, A. M., Mammadov, A. I., Jabarov, S. H., Dubrovinsky, L. S., Liermann, H. P., Morgenroth, W., Mehdiyeva, R. Z., Smotrakov, V. G. & Savenko, B. N. (2015). *Phys. Rev. B*, **92**, 134409.
Lee, N., Vecchini, C., Choi, Y. J., Chapon, L. C., Bombardi, A., Radaelli, P. G. & Cheong, S.-W. (2013). *Phys. Rev. Lett.* **110**, 137203.
Lottermoser, T., Lonkai, T., Amann, U., Hohlwein, D., Ihringer, J. & Fiebig, M. (2004). *Nature*, **430**, 541–544.
Mori-Sánchez, P., Cohen, A. J. & Yang, W. (2008). *Phys. Rev. Lett.* **100**, 146401.
Muñoz, A., Alonso, J. A., Casais, M., Martínez-Lope, M. J., Martínez, J. L. & Fernández-Díaz, M. (2002). *Phys. Rev. B*, **65**, 144423.
Muñoz, A., Alonso, J. A., Casais, M. T., Martínez-Lope, M. J., Martínez, J. L. & Fernández-Díaz, M. T. (2005). *Eur. J. Inorg. Chem.* **2005**, 685–691.
Orobengoa, D., Capillas, C., Aroyo, M. I. & Perez-Mato, J. M. (2009). *J. Appl. Cryst.* **42**, 820–833.
Peintinger, M. F., Oliveira, D. V. & Bredow, T. (2013). *J. Comput. Chem.* **34**, 451–459.
Peng, W., Balédent, V., Chattopadhyay, S., Lepetit, M.-B., Yahia, G., Colin, C. V., Gooch, M. J., Pasquier, C. R., Auban-Senzier, P., Greenblatt, M. & Foury-Leylekian, P. (2017). *Phys. Rev. B*, **96**, 054418.
Perdew, J. P., Ruzsinszky, A., Csonka, G. I., Vydrov, O. A., Scuseria, G. E., Constantin, L. A., Zhou, X. & Burke, K. (2008). *Phys. Rev. Lett.* **100**, 136406.
Perez-Mato, J. M., Orobengoa, D. & Aroyo, M. I. (2010). *Acta Cryst.* A**66**, 558–590.
Petit, S., Balédent, V., Doubrovsky, C., Lepetit, M. B., Greenblatt, M., Wanklyn, B. & Foury-Leylekian, P. (2013). *Phys. Rev. B*, **87**, 140301.
Popov, G., Greenblatta, M. & McCarroll, W. H. (2000). *Mater. Res. Bull.* **35**, 1661–1667.
Poudel, N., Gooch, M., Lorenz, B., Chu, C. W., Kim, J. W. & Cheong, S. W. (2015). *Phys. Rev. B*, **92**, 144430.
Radaelli, P. G. & Chapon, L. C. (2008). *J. Phys. Condens. Matter*, **20**, 434213.
Rault, J. (2014). *Eur. Phys. J. E*, **37**, 113.
Rodríguez-Carvajal, J. (1993). *Physica B*, **192**, 55–69.
Spaldin, N. A. & Fiebig, M. (2005). *Science*, **309**, 391–392.
Wilkinson, C., Sinclair, F., Gardner, P., Forsyth, J. B. & Wanklyn, B. M. R. (1981). *J. Phys. C Solid State Phys.* **14**, 1671–1683.
Yahia, G., Damay, F., Chattopadhyay, S., Balédent, V., Peng, W., Elkaim, E., Whitaker, M., Greenblatt, M., Lepetit, M.-B. & Foury-Leylekian, P. (2017). *Phys. Rev. B*, **95**, 184112.
Yahia, G., Damay, F., Chattopadhyay, S., Balédent, V., Peng, W., Kim, S. W., Greenblatt, M., Lepetit, M.-B. & Foury-Leylekian, P. (2018). *Phys. Rev. B*, **97**, 085128.
Yang, J. & Dolg, M. (2005). *Theor. Chem. Acc.* **113**, 212–224.
Zhao, Z. Y., Liu, M. F., Li, X., Lin, L., Yan, Z. B., Dong, S. & Liu, J. M. (2014). *Sci. Rep.* **4**, 3984.